# 20 dB-enhanced coupling to slot photonic crystal waveguide using multimode interference coupler

Xiaonan Chen, Wei Jiang,[a] Jiaqi Chen, Lanlan Gu, and Ray T. Chen[b]
*Microelectronics Research Center, Department of Electrical and Computer Engineering, The University of Texas at Austin, Austin, Texas 78758*

(Received 18 May 2007; accepted 13 July 2007; published online 28 August 2007)

The authors experimentally demonstrate a slot photonic crystal structure for guiding light in a sub-100-nm-wide low-index region. A multimode interference-based coupling structure is introduced to couple light into such a narrow slot photonic crystal waveguide. A coupler of 1.26 $\mu$m long enhances the coupling efficiency by 20 dB for the quasi-transverse-electric mode over 35 nm optical bandwidth centered at 1562 nm. The measured transmission spectra are in good agreement with the simulated band diagram. © *2007 American Institute of Physics*. [DOI: 10.1063/1.2768640]

Line-defect photonic crystal waveguides (PCWs) with a single guided mode have been incorporated recently in various silicon-based modulator devices,[1–4] where the size of the active region is greatly reduced.[5,6] For electro-optic (EO) material-based active optical components, the unique properties of photonic crystals have been exploited to enhance the nonlinear effect drastically.[7] In order to further enhance the interaction between the light wave and the wave-guiding materials, it is desired to confine light in a narrow active material region, across which a high external electric field can be generated at a low voltage. Slot waveguides[8,9] open the opportunities for guiding and confining light in a sub-100-nm-wide slot filled with low-refractive-index EO materials.[10] Here we embed such nanostructures in photonic crystals and design a slot PCW configuration in order to combine the unusual optical features of photonic crystals and slot waveguides. We also integrate a compact multimode interference (MMI) structure to overcome the difficulties of coupling from a single-mode silicon strip waveguide to a slotted single-mode PCW.

A schematic of the waveguiding structure is depicted in Fig. 1(a). The slotted photonic crystal slab, with high refractive index $n_{Si}=3.48$, is sandwiched between two low-index regions with $n_{SiO_2}=1.46$. With a high index contrast in the vertical direction, such a photonic crystal waveguide supports an in-plane photonic band gap that lies below the light line.[11] Defect modes within the gap region can be created by a great diversity of line defects.[12] Here we introduce the line defect into the photonic crystal slab by replacing a single row of holes with a narrow slot. In addition, we enlarge the width of the defect region to ensure that the guided mode appears near the midgap for robustness against the propagation loss. As a wider defect region may induce multiple bands into the gap region, care must be taken to design the enlarged defect width while maintaining the single-mode operation.[13] We use the three-dimensional (3D) fully vectorial plane-wave expansion (PWE) method to calculate the dispersion diagram of the slot PCW. We assume the hole diameter $d=0.5a$ and the waveguide height $h=0.6a$, where $a=380$ nm is the lattice constant of the photonic crystal. The dispersion diagram plotted in Fig. 1(b) indicates that the slot photonic crystal waveguide retains a single-mode region even when the defect width is enlarged to $1.6W$, where $W=\sqrt{3}a$, as shown in Fig. 1(a). The guided mode is a quasi-transverse-electric (quasi-TE) mode with slow light effect near the band edge.

We then focus on designing the slot width to achieve high mode field amplitude in the low-index slot region. Based on Maxwell's equations, when the transverse electric field component $E_x$ of the quasi-TE mode encounters strong dielectric constant discontinuity of the slot walls, the electric field magnitude jumps to a much higher value on the low-index side.[8] For a slot in a conventional strip waveguide, it has been experimentally demonstrated that the mode field amplitude remains high across the entire slot width if the slot is narrower than the field decay length $1/\gamma_S \sim 4.0a$,[8,9] where $\gamma_S$ is the field decay coefficient in the slot. Based on the same operation principle, we set the slot width of the PCW to $0.25a$ and obtain high $E$-field confinement in the slot, as shown in Fig. 2(a). Simulation of the mode field of the slot PCW is based on the 3D finite-difference time-domain (FDTD) method.

Comparing the mode contour plot of a slot PCW with that of a single-mode silicon strip waveguide in Fig. 2(b), one can identify the evident mode-size and mode-shape mismatches, which will induce significant loss for direct coupling. A conventional solution would be to introduce wave-

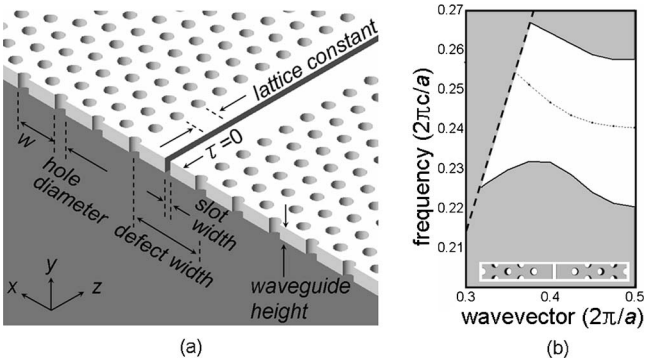


FIG. 1. (a) Line defect structure with a low-index center slot embedded in a photonic crystal slab. (b) Band diagram for a slot photonic crystal waveguide. The thick dashed line is the light line. The gray regions represent the continuum of extended modes. The dotted curve indicates the defect mode. The inset shows the supercell defined in PWE simulation.

[a]Present address: Omega Optics, Inc. Austin, TX 78758.
[b]Electronic mail: raychen@uts.cc.utexas.edu

 

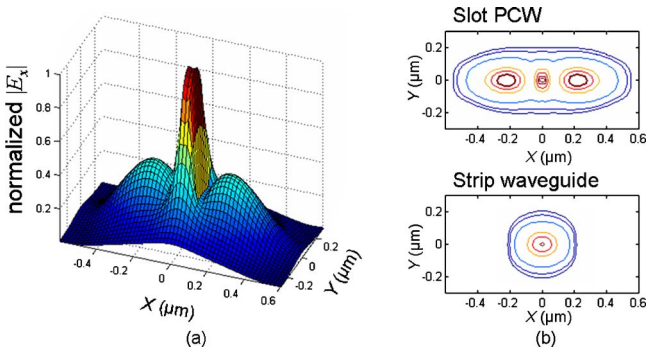


FIG. 2. (Color online) (a) 3D profile of the transverse electric field amplitude of the quasi-TE mode in a slot photonic crystal waveguide, where $a=380$ nm, $d=190$ nm, $h=228$ nm, slot width=95 nm, defect width =1053 nm, $n_{Si}=3.48$, and $n_{slot}=n_{SiO_2}=1.46$. (b) Comparison of two-dimensional field amplitude contours between a slot PCW and a single-mode strip waveguide.

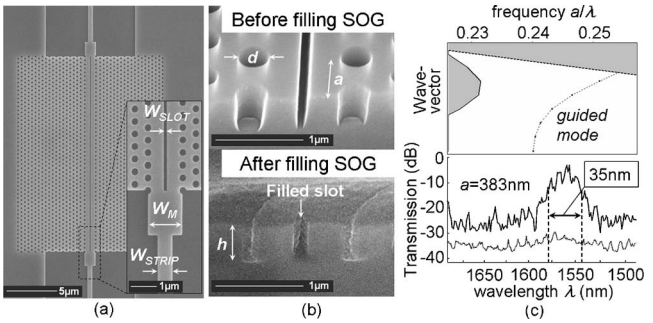


FIG. 4. (a) Scanning electron microscopy top view of a slot PCW integrated with two MMI couplers. The coupling region is enlarged in the inset. (b) Cross-sectionol views of the slot PCW before and after filling SOG. (c) Top panel: enlarged portion of the dispersion diagram for the guided mode. Bottom panel: transmission spectra of a 320 $\mu$m slot PCW with (solid) and without (dashed) the MMI coupler. The spectrum is normalized by the transmission through a reference waveguide.

guide taper structures. However, a taper structure generally requires a taper length of more than several hundred of microns to reduce the propagation loss due to the requirement of adiabatic tapering. In order to implement a more compact mode converter, we integrate multimode interference-based coupling structures in our devices. The basic idea stems from the multimode power splitter structure that has been used to achieve equiphase, balanced power partition from one single-mode input waveguide.[14] A schematic of the multimode interference coupler bridging a strip waveguide and a slot PCW is delineated in the inset of Fig. 3(a). The multimode section is designed to support two even (symmetric) modes with $W_M=1.6W$. The single-mode input waveguide is centered with respect to the multimode section and therefore excites only the symmetric modes. According to the principle of symmetric modal interference in a multimode waveguide,[14] the input mode excites the fundamental and second-order modes with disparate propagation constants; the total field profile is composed of the fundamental mode plus the second-order mode shifted by a certain phase difference.

The phase difference is given by

$$\Delta\sigma=(\beta_0-\beta_2)L_M,$$

where $L_M$ is the length of the multimode section and $\beta_0$ and $\beta_2$ are the propagation constants of the fundamental and second-order modes in the multimode waveguide, respectively. We can therefore adjust $L_M$ to change the phase difference between 0 and $2\pi$ such that the resultant mode profile can best match the slot PCW. With different $L_M$ the coupling efficiency $\eta$ is computed by using the overlap integral between the output field of the multimode section and the guided mode of the slot PCW. As shown in Fig. 3(a), the best coupling efficiency is reached when the phase difference of the even modes in the multimode section is close to $\pi$.

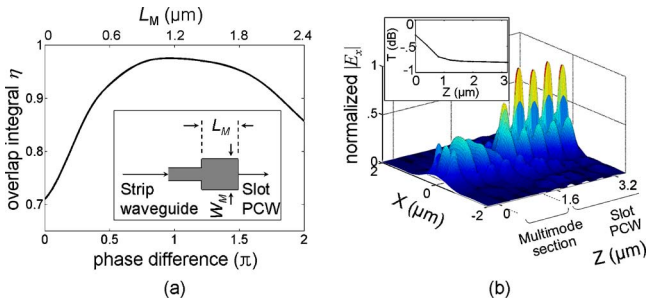


FIG. 3. (Color online) (a) Optimization of the mode overlap integral between the slot PCW and the multimode section. The integral is calculated as a function of the length of the multimode section or the phase difference of the excited even modes. (b) FDTD simulation results: a series of $|E_x(x,y)|$ profiles on the $X$-$Y$ plane imaged at different $Z$ positions. The MMI coupler begins at $Z=0$ $\mu$m and ends at $Z=1.25$ $\mu$m. The inset shows the transmission of the guided quasi-TE mode as a function of the propagation distance.

It has been reported that the coupling efficiency for a PCW also depends on the termination of the photonic crystal waveguide.[15] We simulate the coupling structure with different PCW terminations and the best outcome is obtained when the MMI section interfaces with the slot PCW at the edge of the period which gives termination parameter[15] $\tau=0$, as also indicated in Fig. 1(a). The simulation is based on the 3D FDTD method. Figure 3(b) depicts the evolution of the transverse electric field and optical transmission along the propagation direction. The multimode interference coupler is located between $Z=0$ $\mu$m and $Z=1.25$ $\mu$m. An efficient mode conversion from the conventional silicon strip waveguide to the slot PCW is completed within a 3 $\mu$m distance. The FDTD simulation confirms the total insertion loss induced by mode conversion is less than 1 dB.

Slot photonic crystal waveguides with multimode interference couplers are fabricated on a silicon-on-insulator wafer with a 1 $\mu$m buried oxide layer and a 250 nm top silicon layer. The slot nanostructures are formed in a hexagonal lattice photonic crystal slab with $a=380$ nm and the hole diameter $d=0.5a$. The lattice constant is designed to ensure that the guided mode of the waveguide appears around 1.55 $\mu$m. The waveguide slab layer is patterned using electron-beam lithography followed by reactive ion etching and piranha cleaning. The air holes and the center trench are then filled with spin on glass (SOG). The sample with coated SOG on top is postbaked at 425 °C for 1 h for decarbonization. The refractive index of SOG after hard baking is $n_{SOG}=1.42$, which is close to the value of low-index EO polymers. Figure 4(a) shows a top view of the slot photonic crystal waveguide before filling SOG. The parameters of the waveguide are measured to be $a=383$ nm, $d=207$ nm, $W_{slot}=97$ nm, $W_{strip}=486$ nm, $W_M=1048$ nm, $L_M=1260$ nm, and $h=237$ nm, as indicated in Fig. 4. A cross-sectional view of the waveguide structure shown in Fig. 4(b) confirms that all the void nanostructures in the waveguide slab layer have been filled with SOG. As the last step, an acrylic-based poly-

mer layer that is transparent at 1.55 $\mu$m is coated to reduce the propagation loss due to surface roughness.

To experimentally measure the insertion loss induced by mode mismatch, we integrate a symmetric $1\times2$ power splitter before the slot PCW and introduce a reference arm composed of a strip waveguide to normalize the output of the slot PCW arm. Two samples are fabricated: one sample has MMI couplers at the ends of the slot PCW, the other has the slot PCW directly coupled to the stripe waveguides. The length of the slot photonic crystal waveguides in both cases is 320 $\mu$m. The measured optical spectra are shown in Fig. 4(c). Compared with direct coupling, one can find a 20 dB transmission enhancement over 35 nm optical bandwidth when the coupling structure is employed. The insertion loss for the guided mode is less than 5 dB at the peak wavelength of 1557 nm. The measured band edge appears at a normalized frequency of 0.243 ($\lambda=1576$ nm). The observed spectral range agrees well with the calculated band diagram for the quasi-TE mode of the slot photonic crystal waveguide. The slight frequency discrepancy can be attributed to the dimension and index differences between the simulated and fabricated waveguide structures.

In conclusion, we present a silicon-based slot photonic crystal waveguide and design a multimode interference-based compact mode converter that gives 20 dB higher coupling efficiency for a slot PCW in our experiment. Simulation indicates that this slot photonic crystal waveguide exhibits low group velocity near the band edge and therefore leads to a significant enhancement of nonlinear effect for active devices.[1–6] With proper doping of the left and right silicon regions, a high external field can be generated across the narrow slot with a low voltage. This maximizes the overlap of a high optical mode field and a high external electric field and, together with the low group velocity, provides a promising approach to applying low-index EO materials in highly integrated optical circuits.

This work is supported by AFOSR under Contract No. FA9550-05-C-0171 monitored by G. Pomrenke. Supports from DARPA, the State of Texas, and Sematech are also acknowledged. Nanofabrication and characterization facilities used for this work are partially supported by NSF and SPRING. The authors thank Larry Dalton for helpful discussion.

[1] Y. Jiang, W. Jiang, L. Gu, X. Chen, and R. T. Chen, Appl. Phys. Lett. **87**, 221105 (2005).
[2] Y. A. Vlasov, M. O'Boyle, H. F. Hamann, and S. J. McNab, Nature (London) **438**, 65 (2005).
[3] L. Gu, W. Jiang, X. Chen, and R. T. Chen, IEEE Photonics Technol. Lett. **19**, 342 (2007).
[4] L. Gu, W. Jiang, X. Chen, L. Wang, and R. T. Chen, Appl. Phys. Lett. **90**, 071105 (2007).
[5] M. Notomi, K. Yamada, A. Shinya, J. Takahashi, C. Takahashi, and I. Yokohama, Phys. Rev. Lett. **87**, 253902 (2001).
[6] M. Soljacic, S. G. Johson, S. Fan, M. Ibanescu, E. Ippen, and J. D. Joannopoulos, J. Opt. Soc. Am. B **19**, 2052 (2002).
[7] M. Roussey, M.-P. Bernal, N. Courjal, D. V. Labeke, F. I. Baida and R. Salut, Appl. Phys. Lett. **89**, 241110 (2006).
[8] V. R. Almeida, Q. Xu, C. A. Barrios, and M. Lipson, Opt. Lett. **29**, 1209 (2004).
[9] Q. Xu, V. R. Almeida, R. R. Panepucci, and M. Lipson, Opt. Lett. **29**, 1626 (2004).
[10] B. Bortnik, Y.-C. Hung, H. Tazawa, B.-J. Seo, J. Luo, A. K.-Y. Jen, W. H. Steier, and H. R. Fetterman, IEEE J. Sel. Top. Quantum Electron. **13**, 104 (2007).
[11] E. Chow, S. Y. Lin, S. G. Johnson, P. R. Villeneuve, J. D. Joannopoulos, J.-R. Wendt, G. A. Vawter, W. Zubrzycki, H. Hou, and A. Alleman, Nature (London) **407**, 983 (2000).
[12] S. G. Johnson, P. R. Villeneuve, S. Fan, and J. D. Joannopoulos, Phys. Rev. B **62**, 8212 (2000).
[13] Z. Y. Li, L. L. Lin, and K. M. Ho, Appl. Phys. Lett. **84**, 4699 (2004).
[14] L. B. Soldano and E. C. Pennings, J. Lightwave Technol. **13**, 615 (1995).
[15] Y. A. Vlasov and S. J. McNab, Opt. Lett. **31**, 50 (2006).